Atmos. Chem. Phys. Discuss., 6, 8681–8712, 2006
www.atmos-chem-phys-discuss.net/6/8681/2006/

Atmospheric Chemistry and Physics Discussions

First Odin sub-mm retrievals in the tropical upper troposphere: ice cloud properties

P. Eriksson, M. Ekström, B. Rydberg, and D. P. Murtagh

Department of Radio and Space Science, Chalmers University of Technology, Gothenburg, Sweden

Received: 3 July 2006 – Accepted: 7 August 2006 – Published: 13 September 2006

Correspondence to: P. Eriksson (patrick.eriksson@chalmers.se)

Abstract

There exists today no established satellite technique for measuring the amount of ice in thicker clouds. Sub-mm radiometry is a promising technique for the task, and a retrieval scheme for the first such instrument in space, Odin-SMR, is presented. Several advantages of sub-mm observations are confirmed, such as low influence of particle shape and orientation, and a high dynamic range of the retrievals. In the case of Odin-SMR, cloud ice amounts above ~12.5 km can be determined. The presented retrieval scheme gives a detection threshold of ~4 g/m^2 without saturation even for thickest observed clouds. The main retrieval uncertainty is the assumed particle size distribution. Initial results are found to be consistent with similar Aura MLS retrievals. It is then shown that important differences compared to atmospheric models exist. This first retrieval algorithm is limited to lowermost Odin-SMR tangent altitudes, and further development should improve the detection threshold and the vertical resolution.

1 Introduction

A main uncertainty for prediction of the future climate is the poor understanding cloud processes (IPCC, 2001), where clouds in the tropical upper troposphere are of particular concern. This, as the radiative fluxes are the largest in the tropical region, clouds at high altitudes have the strongest influence on outgoing longwave radiation (Okhert-Bell and Hartmann, 1992) and the response of such clouds to changing surface temperatures is unclear (see e.g. Genio and Kovari, 2002). Further these clouds are most likely a key factor for upward transport of air into the stratosphere (Corti et al., 2006), a phenomenom not completely understood.

A better treatment of clouds in atmospheric modelling requires improved satellite observations, but even to provide accurate data for such a basic parameter as the ice water content (IWC) is a challenging task. In rough terms, a remote sounding measurement of cloud ice will primarily be sensitive to particles having a size similar

ACPD
6, 8681–8712, 2006

to the wavelength used. This means that a single-wavelength observation will only "sample" a smaller fraction of the possible particle size range (about 10^{-6}–10^{-2} m). To deduce an IWC value from this observation requires thus assumptions on the relative amount of particles at different sizes, the particle size distribution (PSD). The problem is that the PSD is not a constant quantity, and varying data have also been obtained from in-situ measurement campaigns (Heymsfield and Platt, 1984; McFarquhar and Heymsfield, 1997; Heymsfield et al., 2002).

An ideal sensor for cloud ice measurements would accordingly perform observations over a wide range of wavelengths, but such an instrument is yet a hope for the future. To make things worse, present satellite techniques operate at the far ends of the interesting wavelength range, either in the optical/thermal-IR region (e.g. Winker and Trepte, 1998; Stubenrauch et al., 1999) or the mm-wave range (e.g. Hong et al., 2005; Wu et al., 2005). This should be compared to suggestions for dedicated cloud ice instruments where the core part is a sub-mm radiometer (Evans et al., 2002), though preferably complemented with mm and IR channels. The focus on the sub-mm range for cloud ice sounding is a consequence of that good cloud penetration capability and sensitivity to most important particle size range can be combined (Evans et al., 1998).

The sub-mm radiometer (SMR) on-board the Odin satellite was launched in 2001 and became then the first satellite instrument for atmospheric sounding in this wavelength region (Murtagh et al., 2002). Odin-SMR is a limb sounder and software for rigorous simulations of this observation geometry including polarised scattering has first recently been developed (Emde et al., 2004a). This development now enables cloud ice signatures in Odin-SMR tropospheric spectra to be quantified, and a first retrieval scheme is presented here. The atmospheric opacity sets a lower limit for Odin-SMR around 10 km and the retrieval is restricted to the upper tropical troposphere.

A second sub-mm limb sounder is now in space, Aura MLS launched in 2004. Cloud ice retrievals from this instrument have already been presented but then only using mm-wave data, from 230 GHz (Li et al., 2005; Wu et al., in press). This instrument has also a 640 GHz radiometer, while the Odin-SMR data used here are from 501 and

544 GHz. These sub-mm limb sounders will give valuable data sets, to e.g. constrain climate models and to support the analysis of dedicated cloud missions, such as the CloudSat 94 GHz cloud profiling radar (Stephens et al., 2002).

2 The Odin satellite

2.1 Overview

The Odin mission is a collaboration between Sweden, Canada, France and Finland, with the launch of the satellite in February 2001 (Nordh et al., 2003). The observation time is divided on equal terms between astronomy and atmospheric science objectives. The satellite carries two instruments, a sub-mm radiometer package (SMR) and an optical spectrograph and infrared imager system (OSIRIS). The SMR instrument is used for both astronomy and atmospheric observations, while OSIRIS is only operated during the atmospheric part (Murtagh et al., 2002).

The limb scanning of Odin is performed by rotating the complete satellite, with a rate giving a vertical movement of the tangent point of about 750 m/s. Spectra are taken during both downward and upward scanning, with the lower turning point at a nominal altitude of 6 km. The integration time is 0.875 s and subsequent spectra are recorded every 2 s. These values are changed to 1.875 and 4 s, respectively, for shorter periods to avoid overflow of onboard memory capacity. The near polar orbit is sun-synchronous, with an altitude of about 600 km and ascending node around 18.00.

2.2 The data

This study is based solely on data from the SMR receiver (Frisk et al., 2003). The four front-ends of SMR give together sensitivity tunable over 486.1–503.9 and 541.0–581.4 GHz, while spectrometer and data rate constraints set a limit at about 1.6 GHz for the instantaneous overall bandwidth. SMR is then operated in several observation

ACPD
6, 8681–8712, 2006

modes to cover all molecular transitions of interest. The data used here are taken from the most frequently used mode, the stratospheric mode, which aims at retrieving ClO, N_2O, HNO_3 and O_3. The stratospheric mode consists of two bands, at 501 and 544 GHz. Relevant spectroscopic features of these bands are shown in Fig. 1. SMR is a single sideband receiver. See Urban et al. (2005) for further details and a description of the standard processing.

The basic observation schedule gives stratosphere mode data every third day, but the data set is more dense during the Decembre–May period due to observation campaigns focusing on Arctic winter polar research. For these first retrievals only spectra for tangent altitudes below 9 km are considered (Sect. 4.2). This means that used data are grouped around the scan turning points, where the groups consist of 3–8 spectra. The closest horizontal distance between subsequent spectrum groups is 1000 km. Example on data values are found in Fig. 2.

The response of the SMR receivers is linearly polarised. The mounting is such that the response corresponds to a $\pm 45^{\circ}$ polarisation in atmospheric coordinates. The consequences of this fact are discussed in Sect. 3.2.

3 Radiative transfer

3.1 Software

Radiative transfer simulations were performed with version 1.1 of the Atmospheric Radiative Transfer Simulator (ARTS). This is a development version of ARTS-1 (Buehler et al., 2005), where features needed for rigorous simulations of scattering in limb sounding geometry have been added. Polarisation effects are fully considered, where the polarisation state is expressed by the Stokes formalism. The geoid and the surface can have arbitrary shape, and atmospheric fields can have variations in all three dimensions. Scattering by molecules and aerosols can be neglected for sub-mm radiation, and this is reflected in ARTS-1.1 such that the scattering calculations can be restricted

to a smaller part of the model atmosphere. Two modules for the treatment of scattering exist, a discrete ordinate iterative method (Emde et al., 2004a) and a reverse Monte Carlo algorithm (Davis et al., 2005a). Particle properties for single scattering are calculated externally, where the T-matrix code of Mishchenko and Travis (1998) was applied for this study. Figure 1 shows that Odin-SMR spectra with evident scattering signatures can be recreated in detail by simulations, a fact that gives high confidence in the performance in ARTS-1.1.

3.2 Simulation set-up

Spectroscopic data were taken from the retrieval of stratospheric gas species (Urban et al., 2005). Pure clear-sky calculations were performed in a 2-D mode, with temperatures and geometrical altitudes from ECMWF and gaseous vertical profiles from the SMR a priori climatology as described in Ekström et al. (2006). The vertical variation of the antenna response and the frequency response of the spectrometer were considered for the clear-sky part. These effects were ignored for scattering calculations, as tests showed that this allowed much more rapid calculations with negligible impact on final results. The contribution from the image sideband can be neglected for considered range of tangent altitudes as both sidebands exhibit very similar radiances for the considered range of tangent altitudes.

A spherically symmetric atmosphere (1-D) was assumed when determining the cloud induced change in brightness temperature. The calculations were performed by the method of Emde et al. (2004a), but some Monte Carlo simulations were also made for validation purposes. Different shapes of the ice particles were considered, as described in Sect. 4.3. The particle orientation was assumed to be either completely random or azimuthally random. No ±45° or circular polarisation (Stokes components 3 and 4) are generated for these conditions and it is sufficient to only consider the first two Stokes components in the simulations. This theoretically based statement was confirmed by simulations. A consequence of this fact is that the signal recorded by SMR correspond to the mean of the intensity for vertical and horizontal polarisation,

here equal to the first Stokes element, as long as no esoteric particle orientation occurs in the atmosphere.

3.3 Impact of scattering

Compared to the corresponding clear-sky case, cloud ice scattering can cause both increased and decreased radiances in mm and sub-mm limb sounding measurements. The sign of the effect depends on the vertical variation of gaseous absorption, cloud altitude and tangent altitude (see Emde et al., 2004b for simulation results and Wu et al., 2005 for observation evidence). Increased radiances are primarily found where both cloud top and tangent altitudes are high, while for the measurement geometry used here cloud scattering give decreased brightness temperatures throughout, as also indicated by Figs. 1–2. This is the case as only cloud ice well above the tangent point has a significant influence, and the averaged emission scattered into the line-of-sight has a lower intensity than the "warm" emission coming from the region around the tangent point that it replaces. The impact of lower cloud ice is screened out by high gaseous absorption.

4 Retrieval algorithm

4.1 Basic considerations and approach

This first Odin-SMR cloud ice retrieval scheme uses only spectra with tangent altitudes below 9 km. There are several reasons to start with this part of the data set. First of all, the largest signatures of cloud scattering are found for these tangent altitudes (up to 100 K, see Fig. 2). In addition, the effect of cloud scattering is here consistently a decrease in measured intensity (Sect. 3.3), which simplifies the analysis. In Ekström et al. (2006) it is further shown that very few quantities have a significant influence on these spectra (temperature, humidity and scattering). It is further explained that un-

certainties in instrument responses (such as sideband filtering and antenna response) can be neglected.

Odin-SMR is a limb sounder, but the measurement principle applied here is more of down-looking character. This is the case as high absorption below 9 km removes all influence of the most distant part of the limb view. The region around the tangent point acts practically as a blackbody. This yields many similarities with the dedicated sub-mm cloud ice measurements proposed in Evans et al. (2002), using the lower part of the troposphere as a blackbody background. There are though some important differences. The high incidence angles here give sensitivity to only higher altitudes, and the mean particle size can not be determined as the two channels used (501 and 544 GHz) are too close in wavelength to provide useful information.

The measurement principle is then as follows. The measured emission intensity is, for clear-sky conditions, governed by temperature and humidity. Clouds along the line-of-sight at sufficient altitude (above ∼11 km for 501 GHz and ∼13 km for 544 GHz) and with particles large enough to cause scattering at these wavelengths, will result in a decrease in the observed brightness temperature, T_b. The first step of the retrieval is to determine the cloud induced T_b depression, and the second step is to map the depression to a cloud ice amount. The unknown vertical extension of the cloud causes a retrieval ambiguity that can be partly handled by combining information from 501 and 544 GHz. Each pair of 501/544 GHz spectra is treated individually and each cloud retrieval represents a horizontal area ∼3 km wide in west-east direction, and ∼100 km long in north-south direction.

4.2 Determination of cloud signal

The cloud signal is defined as the T_b depression compared to corresponding clear-sky case, here shorten to ΔT_b. The determination of clear-sky radiances is based on the parallel humidity retrieval, described in the accompanying paper by Ekström et al. (2006). In short, Odin-SMR spectra are generated for different assumed relative humidities, and this set of simulations are used to map measured T_b value to a

humidity. The simulations are performed in a 2-D mode and full account of gradients in atmospheric temperatures (from ECMWF) is taken. A detailed investigation made it possible to compensate for a small systematic calibration error, but also revealed a ∼2 K random component that is directly translated to an identical uncertainty in ΔT_b.

The T_b depression is here taken as the difference between measured T_b and simulated value for 120 %RHi. It could be argued that 100 %RHi or the humidity retrieved in Ekström et al. (2006) are better choices for the reference level, but this question has small practical concern. The corresponding ΔT_b uncertainty is ∼1 K. The level 120 %RHi was selected to obtain a more conservative estimate of the cloud detection frequency.

4.3 Impact of microphysical parameters

As mentioned, the measurements can not be used to confine the mean particle size and this has the consequence that a particle size distribution (PSD) must be assumed. The PSD of McFarquhar and Heymsfield (1997) (hereafter MH97) is commonly used for tropical conditions and it is also used here as best estimate on the mean tropical PSD.

The Odin-SMR measurements can not give any firm upper limit on ice amounts. This is the case as the ice amount in principle can be infinite as long as all particles sizes are sufficiently small that no scattering effects appear at the sub-mm wavelengths employed. On the other hand, a lower limit on cloud ice amount can be given by assuming that the particle size is such that a maximum scattering impact, for a fixed ice amount, is obtained. Simulations showed that a mono-dispersive PSD at ∼200 µm fulfils this criterion. Any real PSD will have some width and as a more realistic option a gamma distribution peaking at 200 µm was selected. The width parameter of the gamma PSD was set to 4. This corresponds to the most narrow PSD that is consistent with width values reported by Heymsfield (2003). The MH97 and gamma PSDs are compared in Fig. 3. The importance of assumed PSD on the mapping between ΔT_b and cloud ice amounts is shown in Fig. 4.

The influence of particle shape was studied by considering different spheroidal shapes, with aspect ratios between 1 and 3.5. An aspect ratio >1 means that the horizontal length exceeds the vertical extent. ARTS (Sec. 3.1) allows two options for particle orientation, randomly oriented and horizontally aligned. The later option implies random azimuthal orientation. Results for different combinations of aspect ratio and particle orientation are shown in Fig. 5. For an aspect ratio of 1 there is no difference between the two orientation options. No discernable variation was found for different aspect ratios as long as randomly oriented particles are assumed, and those results are not included in Fig. 5. A polarisation dependent impact of aspect ratio is though found for horizontally aligned particles. The polarisation dependency is shown in Fig. 5 for an aspect ratio of 3.5. Odin-SMR corresponds to the dashed curve (mean of I_v and I_h, see Sects. 2.2 and 3.2), which in this context is the most advantageous case as the mapping between ΔT_b and ice amount is more affected by aspect ratio assumed for vertical and horizontal polarisation.

However, an aspect ratio value of 3.5 was included mainly for matters of illustration, and values of 1–2 should be more representative for atmospheric conditions. This as the overall ensemble aspect ratio should not in general deviate strongly from 1 (A. J. Heymsfield, private communication). A mean aspect ratio of 1.2 was also found in an investigation of 122 GHz MLS data (Davis et al., 2005b). The judgement must then be that incorrect assumptions on particle shape and orientation should only cause marginal retrieval errors. Spherical particles are assumed throughout below.

4.4 Impact of cloud thickness and altitude

The T_b depression caused by a given ice amount depends on the cloud altitude. The altitude variation is mainly governed by the absorption properties at the frequency considered, and thus differs between the 501 and 544 GHz bands. The general principle is that a high cloud, where the gaseous absorption is smaller, gives a higher ΔT_b for a given ice amount. This is illustrated in Fig. 6 for 501 GHz. The ice is, here and elsewhere in the study, evenly distributed in the cloud layer. The gamma PSD is used for

this comparison to avoid that the PSD changes with altitude (through the temperature dependency of MH97).

The 501 GHz band has low absorption above ∼14 km and accordingly the mapping is relatively constant for cloud altitudes above this altitude, while a large difference is seen in comparison to an altitude of e.g. 12 km. The absorption in the 544 GHz band extends to higher altitudes and the cloud altitude influences the mapping up to ∼16 km.

The altitude variation of the cloud influence means that the cloud thickness must also be considered, but simulations showed that the cloud thickness is of less importance if an adaptive definition of the cloud altitude is introduced. It was found that for thin clouds the impact of cloud thickness can be neglected if the centre point of the cloud layer is kept constant. The same is achieved for thick clouds if the top altitude is considered instead. These features are illustrated by the 13/3 km case in Fig. 6, that follows closely 13/1 km for weak clouds and asymptotically approaches 14/1 km for strong clouds. That is, the term cloud altitude will be defined as the the centre point for clouds with low ice amounts, and gradually move towards the top altitude for increasing ice columns. The effective altitude for the highest cloud columns encountered here should be 100–200 m below the cloud top altitude. The definition of the cloud top must though be taken as the highest altitude with particles large enough to influence sub-mm radiation, that probably can differ substantially from the optically determined cloud top.

4.5 Mapping to partial ice column

The band at 501 GHz is sensitive to clouds down to ∼11 km (Fig. 6), while for 544 GHz the sensitivity starts at ∼14 km (not shown). The higher absorption at 544 GHz implies that for all realistic cases the ΔT_b will be higher for 501 GHz than for 544 GHz, despite a higher scattering cross-section at the higher frequency (60% if Rayleigh scattering is assumed). The 501 GHz band is then the primary band for cloud detection and retrievals.

However, the retrieval can not be based on 501 GHz solely as the unknown cloud altitude would then cause a very high retrieval error. For example, a 501 GHz ΔT_b of

20 K can either be a ~200 g/m^2 cloud at 11 km or a ~1 g/m^2 cloud at 15 km (Fig. 6). By incorporating 544 GHz data this ambiguity can be decreased strongly. In simple terms, if no T_b depression is found for 544 GHz the cloud altitude is below 14 km, and vice versa. For clouds above 14 km the relative size in ΔT_b at 501 and 544 GHz enables a relatively accurate determination of the cloud altitude.

The retrieval scheme is described more in detail by Fig. 7. The figure confirms the discussion above. For example, it shows that altitude ambiguity can be handled above 14 km by combining information from 501 and 544 GHz. The ice amount in clouds at lower altitudes is retrieved assuming a cloud altitude between 13.5 and 14 km. The mapping for 13.5 km is marked as NaN km in Fig. 7 to indicate that the cloud altitude can not be determined here. The 544 GHz ΔT_b is used as an indicative weighting between 13.5 and 14 km. If the real cloud altitude is lower, this gives an underestimation of the cloud ice. This behaviour corresponds to a lower retrieval response to ice below 14 km. The retrieval has thus an altitude dependent response, which is estimated in Fig. 8. The altitude response was obtained by comparing ice-depression mapping curves for different cloud altitudes (Fig. 6), evaluated for a 501 GHz ΔT_b of 50 K. This estimate should represent average conditions, but it shall be noted that the altitude response is not a constant quantity. A higher ΔT_b value corresponds to a lower response to cloud ice at lower altitudes. This simply as very high ΔT_b values can not be obtained with cloud altitudes around e.g. 11 km.

This Odin-SMR cloud ice retrieval is thus an estimate of a partial cloud ice column, with an altitude response given by Fig. 8. The response of 0.5 is found at ~12.5 km and this altitude is used when a lower altitude for the column value must be specified.

Figures 4–8 are all valid for a tangent altitude of 7 km. Mappings and response are very similar for other considered tangent altitudes.

5 Results

The main objective of the paper is to present the retrieval methodology and only example results are given, to indicate the quality and potential usage of the Odin-SMR data set. More detailed investigations are left for forthcoming publications. Mean results for the December 2001–August 2004 period are shown, following Ekström et al. (2006).

5.1 Cloud detection frequency

A cloud is considered as detected if the 501 GHz ΔT_b exceeds some specified value. The threshold value shall be as small as possible without including a significant number of false cloud detections due to uncertainties in estimated ΔT_b. The main ΔT_b uncertainty is the random calibration error discussed in Sect. 4.2. For example, the data points in Fig. 7 above the 16 km curve (with low depression values for both bands) are primarily an effect of the random calibration error, and shall not be taken as detections of high altitude clouds. There exists a similar uncertainty for the 501 GHz ΔT_b but has been shown to be of smaller size, more precisely to have a 1σ variation of 2 K. Considering this uncertainty, 5 K is used as threshold for the cloud detection frequency. This threshold value corresponds to an ice column of about 4 g/m^2 (Fig. 7). Such an ice water path has an optical zenith opacity in the order of 0.2 (Heymsfield et al., 2003)

The mean cloud detection frequency obtained for the time period considered is shown in Fig. 9. Somewhat higher cloud frequencies are obtained for lower ΔT_b threshold values, but the geographical pattern is not changed. The mean difference between a threshold of 2 and 5 K was determined to 0.03, and this can be taken as a general error estimate for Fig. 9.

The fact that the cloud detection frequency is close to zero over substantial areas, at expected geographical positions, is a strong confirmation of the claim that the 501 GHz ΔT_b is determined with the precision of ~2 K.

ACPD
6, 8681–8712, 2006

5.2 Partial cloud ice columns

The 501 and 544 GHz ΔT_b values obtained are mapped to partial cloud ice columns in the manner described in Sect. 4.5. The cloud ice column is normally denoted as the ice water path (IWP). All measurements with 501 GHz ΔT_b below 2 K are treated as cloud free. A lower limit for IWP is obtained by assuming a 200 µm gamma PSD (Sect. 4.3), while most probable values are based the MH97 PSD. Mean IWP fields for the time period considered are shown in Fig. 10, together with data from atmospheric models for comparison reasons. The vertical distributions of cloud ice water content in ECMWF and ECHAM were weighted with the response established for Odin-SMR (Fig. 8) to obtain directly comparable quantities. ECMWF is a model for numerical weather prediction and assimilates both satellite and in-situ measurements, while ECHAM is a pure climate model (GCM) and ice field shown does not represent a particular time period.

The relative difference between minimum and MH97 estimates decreases with increasing IWP (Fig. 3), to be about 2 for thickest clouds. The minimum IWP fields in Fig. 10 is a factor 2–5 lower than corresponding MH97 results, for areas with mean IWP >2.5 g/m^2. The 200 µm gamma PSD has low probability to be found in practice and true IWP values should accordingly be considerable higher than reported minimum estimates. Despite this, the minimum estimates are found to be larger than the ECHAM data, and be very similar to ECMWF, above central Africa. The minimum estimates are also of the same magnitude as the model data over S. America. Odin-SMR retrievals based on MH97 are also significantly above the ECMWF and ECHAM for these regions. It shall here be noted that Odin-SMR does not sample the full diurnal cycle (tropical latitudes are passed at around 06.00 and 18.00 local time) and this effect has not been considered in the comparison to ECMWF and ECHAM.

The Odin-SMR and atmospheric model results show better agreement over the oceans, with highest values in areas of strong convection. Odin-SMR tends to place the highest IWP values in more localised areas, but this can be an effect of the limited size of the Odin-SMR data set.

ACPD
6, 8681–8712, 2006

Li et al. (2005) present a comparison between Aura MLS cloud ice retrievals, ECMWF and a number of global climate models (ECHAM not included). If ECMWF is used as a common reference, there appear to be a high consistency between Aura MLS and Odin-SMR cloud ice retrievals. For example, notable differences between retrieved and model data above Africa and S. America were also found by Li et al. (2005). An important aspect is that the MLS retrievals are also based on the MH97 PSD. A closer comparison to Aura MLS is left for future work.

The dominating error source of the IWP retrieval is the assumed PSD. A detailed error analysis would require access and analysis of large data sets of in-situ measurements, spanning all relevant atmospheric conditions. Such data are not at hand and only rough estimates can be given. An initial study (Rydberg, 2004) compared total scattering extinction for different PSDs. Focus is here given to the comparison to the PSD of Donovan (2003), here denoted as D03, despite it is determined for mid-latitude conditions. This as the D03 PSD is based on remote sensing data, and should then be totally independent in technical aspects to MH97, derived from in-situ measurements. In addition, D03 incorporates radar data that should give a good constrain for the particle size range of concern for sub-mm observations. It was found that replacing MH97 with D03 should change the IWP with less than 25%, if the cloud ice is found at temperatures around –40 °C. On the other hand, large differences between MH97 and D03 (and the two other considered PSDs) were noted for lower temperatures (–60 °C), that correspond to IWP retrieval errors >100 %, but it can be questioned that if the D03 PSD is valid for such temperatures. Considering this discussion and found ratios between minimum and most probably estimate, a value of 50% is here adopted as a general estimate of the IWP retrieval accuracy.

This high retrieval uncertainty originates in the fact that any remote sensing technique limited to a single wavelength range will only be sensitive to a part of all cloud ice particles, where short wavelengths will give sensitivity to small particles, and vice versa. If the purpose is to estimate the ice mass, the used wavelength should then be selected in such way that highest sensitivity is given to the particle size region hold-

ing the main part of the total mass. Figure 11 shows the mass distribution for some conditions representing thinner and thicker clouds at temperatures found in the upper tropical troposphere. The size range of interest differs somewhat between the cases, but a dominating part of the ice mass is found in particles having a diameter of 35–400 µm throughout. The maximum sensitivity of Odin-SMR at 200 µm (Sect. 4.3) is centrally placed in this size range. This discussion indicates that, despite that the IWP retrievals presented are estimated to have important uncertainties, the situation is not better for retrievals using other wavelength regions.

6 Conclusions

A first cloud ice retrieval scheme for Odin-SMR has been developed. Observation data are taken from the two bands of the stratospheric mode, 501 and 544 GHz, where so far only spectra with tangent altitudes below 9 km are considered. The first step of the retrieval is to determine, for each band, the brightness temperature depression (ΔT_b) induced by ice clouds, compared to the corresponding clear-sky situation. This step is based on the work of Ekström et al. (2006). For the purpose of cloud detection a simple ΔT_b threshold is applied. The main limiting factor for the cloud detection is a random calibration error causing a 2/3 K uncertainty for the 501/544 GHz ΔT_b.

The measurements allow also retrieval of the ice water path (IWP) above ~12.5 km. As Odin-SMR is used here more in the sense as a down-looking instrument rather than as a limb sounder, information from 501 and 544 GHz must be combined. The 501 GHz band exhibits the strongest cloud signal, and the practical contribution of the 544 GHz data is to constrain the cloud altitude. The sensitivity is such that there is a full response to cloud ice above 14 km, but decreasing below to reach zero at 11.5 km. The detection threshold corresponds to a IWP of ~4 g/m^2. The dynamic range of the retrievals extends up to at least 450 g/m^2. The largest observed IWP values are estimated to ~600 g/m^2. The dominating error source for the IWP retrieval is that a particle size distribution (PSD) must be assumed. A detailed error analysis is not

possible, as data to evaluate the validity of assumed PSD for different conditions are lacking, and at this point retrieval errors exceeding 50% can not be excluded.

A firm lower limit for the retrieved cloud ice column can be obtained by assuming a PSD that maximises the scattering cross-section for wavelengths used. The difference between minimum and best estimate decreases with increasing IWP. For the areas with thicker ice clouds, the minimum estimate of mean IWP is a factor 2–5 below the most probable value.

A simple comparison to the ice fields in ECMWF and the ECHAM GCM is made, that gives consistent results with a similar comparison involving Aura MLS (Li et al., 2005). Both the Odin-SMR and Aura MLS retrievals indicate that atmospheric models show tendencies to underestimate the amount of cloud ice. For example, already the minimum Odin-SMR IWP over central Africa is above the GCM data. However, the high retrieval uncertainties so far limit a more detailed investigation of the performance of the models. Other existing satellite data are however not better in this respect. On the contrary, sub-mm radiometry is an advantageous approach for measuring cloud ice contents, but Odin-SMR lacks the broad coverage of the mm/sub-mm region that should be used by a dedicated cloud ice instrument (Evans et al., 2002).

It has been shown that the impact of scattering on Odin-SMR spectra is understood, and valuable climate data can be extracted. This justifies continued effort to also make use of the cloud ice information found in spectra with higher tangent altitudes. Such a development should result in a higher sensitivity to clouds with low IWP values and an improved vertical resolution.

Acknowledgements. This work is based in various ways on efforts made by persons inside the Odin-SMR retrieval group. Essential contributions by the ARTS community are also acknowledged. ECMWF and ECHAM data were generously provided by A. Tompkins and U. Lohmann, respectively. Financial support was provided by the Swedish Space Board and the Swedish National Graduate school of Space Technology.

References

Buehler, S. A., Eriksson, P., Kuhn, T., von Engeln, A., and Verdes, C.: ARTS, the Atmospheric Radiative Transfer Simulator, J. Quant. Spectrosc. Radiat. Transfer, 91, 65–93, doi:10.1016/j.jqsrt.2004.05.051, 2005. 8685

Corti, T., Luo, B. P., Fu, Q., Vömel, H., and Peter, T.: The impact of cirrus clouds on tropical troposphere-to-stratosphere transport, Atmos. Chem. Phys., 6, 2539–2547, 2006. 8682

Davis, C., Emde, C., and Harwood, R.: A 3D polarized reversed Monte Carlo radiative transfer model for mm and sub-mm passive remote sensing in cloudy atmospheres, IEEE Trans. Geosci. Remote Sensing, 43, 1096–1101, 2005a. 8686

Davis, C. P., Wu, D. L., Emde, C., Jiang, J. H., Cofield, R. E., and Harwood, R. S.: Cirrus induced polarization in 122 GHz Aura Microwave Limb Sounder radiances, Geophys. Res. Lett., 32, L14806, doi:10.1029/2005GL022681, 2005b. 8690

Donovan, D. P.: Ice-cloud effective particle size parameterization based on combined lidar, radar reflectivity, and mean Doppler velocity measurements, J. Geophys. Res., 108(D18), 4573, doi:10.1029/2003JD003469, 2003. 8695

Ekström, M., Eriksson, P., Rydberg, B., and Murtagh, D.: First Odin sub-mm retrievals in the tropical upper troposphere: Humidity and cloud ice signals, Atmos. Chem. Phys. Discuss., 6, 8649–8680, 2006. 8686, 8687, 8688, 8689, 8693, 8696

Emde, C., Buehler, S. A., Davis, C., Eriksson, P., Sreerekha, T. R., and Teichmann, C.: A polarized discrete ordinate scattering model for simulations of limb and nadir longwave measurements in 1D/3D spherical atmospheres, J. Geophys. Res., 109(D24), D24207, doi:10.1029/2004JD005140, 2004a. 8683, 8686

Emde, C., Buehler, S. A., Eriksson, P., and Sreerekha, T. R.: The effect of cirrus clouds on limb radiances, J. Atmos. Res., 72, 383–401, doi:10.1016/j.atmosres.2004.03.023, 2004b. 8687

Evans, K. F., Walter, S. J., Heymsfield, A. J., and Deeter, M. N.: Modeling of submillimeter passive remote sensing of cirrus clouds, J. Appl. Meteorol., 37, 184–205, 1998. 8683

Evans, K. F., Walter, S. J., Heymsfield, A. J., and McFarquhar, G. M.: Submillimeter-wave cloud ice radiometer: Simulations of retrieval algorithm performance, J. Geophys. Res., 107, 2.1–2.21, 2002. 8683, 8688, 8697

Frisk, U., Hagström, M., Ala-Laurinaho, J., Andersson, S., Berges, J. C., Chabaud, J. P., Dahlgren, M., Emrich, A., Florén, H. G., Gredrixon, M., Gaier, T., Haas, R., Hirvonen, T., Hjalmarsson, A., Jakobsson, B., Jukkala, P., Kildal, P. S., Kollberg, E., Lassing, J., Lecacheux,

A., Lehikoinen, P., Lehto, A., Mallat, J., Marty, C., Michet, D., Narbonne, J., Nexon, M., Olberg, M., Olofsson, A. O. H., Olofsson, G., Origné, A., Petersson, M., Piironen, P., Pons, R., Pouliquen, D., Ristorcelli, I., Rosolen, C., Rouaix, G., Räisänen, A. V., Serra, G., Sjöberg, F., Stenmark, L., Torchinsky, S., Tuovinen, J., Ullberg, C., Vinterhav, E., Wadefalk, N., Zirath, H., Zimmermann, P., and Zimmermann, R.: The Odin satellite I. Radiometer design and test, Astron. Astrophys., 402, L27–L34, doi:10.1051/0004-6361:20030335, 2003. 8684

Genio, A. D. D. and Kovari, W.: Climatic properties of tropical convection under varying environmental conditions, J. Climate, 15, 2597–2615, 2002. 8682

Heymsfield, A. J.: Properties of tropical and midlatitude ice cloud particle ensembles, Part II: Applications for mesoscale and climate models, J. Atmos. Sci., 60, 2592–2611, 2003. 8689

Heymsfield, A. J. and Platt, C. M. R.: A parameterization of the particle size spectrum of ice clouds in terms of the ambient temperature and the ice water content, J. Atmos. Sci., 41, 846–855, 1984. 8683

Heymsfield, A. J., Bansemer, A., Field, P. R., Durden, S. L., Stith, J. L., Dye, J. E., Hall, W., and Grainger, C. A.: Observations and parameterizations of particle size distributions in deep tropical cirrus and stratiform precipitating clouds: Results from in situ observations in TRMM field campaigns., J. Atmos. Sci., 59, 3457–3491, 2002. 8683

Heymsfield, A. J., Matrosov, S., and Baum, B.: Ice water path - optical depth relationships for cirrus and deep stratiform ice cloud layers, J. Appl. Meteorol., 42, 1369–1390, 2003. 8693

Hong, G., Heygster, G., Miao, J., and Kunzi, K.: Detection of tropical deep convective clouds from AMSU-B water vapor channels measurements, J. Geophys. Res., 110, D05205, doi:10.1029/2004JD004949, 2005. 8683

IPCC: Climate change 2001: The scientific basis, Cambridge University Press, Cambridge, UK, 2001. 8682

Li, J. L., Waliser, D. E., Jiang, J., Wu, D. L., Read, W., Waters, J. W., Tompkins, A. M., Donner, L. J., Chern, J. D., Tao, W. K., Atlas, R., Gu, Y., Liou, K. N., Genio, A. D., Khairoutdinov, M., and Gettelman, A.: Comparisons of EOS MLS cloud ice measurements with ECMWF analyses and GCM simulations: Initial results, Geophys. Res. Lett., 32, L18710, doi:10.1029/2005GL023788, 2005. 8683, 8694, 8695, 8697

McFarquhar, G. M. and Heymsfield, A. J.: Parameterization of tropical cirrus ice crystal size distribution and implications for radiative transfer: Results from CEPEX, J. Atmos. Sci., 54, 2187–2200, 1997. 8683, 8689, 8704

Mishchenko, M. I. and Travis, L. D.: Capabilities and limitations of a current FORTRAN imple-

mentation of the T-matrix method for randomly oriented rotationally symmetric scatterers, J. Quant. Spectrosc. Radiat. Transfer, 60, 309–324, 1998. 8686

Murtagh, D., Frisk, U., Merino, F., Ridal, M., Jonsson, A., Stegman, J., Witt, G., Eriksson, P., Jiménez, C., Megie, G., de La Noë, J., Ricaud, P., Baron, P., Pardo, J. R., Hauchcorne, A., Llewellyn, E. J., Degenstein, D. A., Gattinger, R. L., Lloyd, N. D., Evans, W. F. J., McDade, I. C., Haley, C., Sioris, C., von Savigny, C., Solheim, B. H., McConnell, J. C., Strong, K., Richardson, E. H., Leppelmeier, G. W., Kyrölä, E., Auvinen, H., and Oikarinen, L.: An overview of the Odin atmospheric mission, Can. J. Phys., 80, 309–319, 2002. 8683, 8684

Nordh, H. L., von Schéele, F., Frisk, U., Ahola, K., Booth, R. S., Encrenaz, P. J., Hjalmarson, A., Kendall, D., Kyrölä, E., Kwok, S., Lecacheux, A., Leppelmeier, G., Llewellyn, E. J., Mattila, K., Mégie, G., Murtagh, D., Rougeron, M., and Witt, G.: The Odin orbital observatory, Astron. Astrophys., 402, L21–L25, doi:10.1051/0004-6361:20030334, 2003. 8684

Okhert-Bell, M. E. and Hartmann, D. L.: The effect of cloud type on earth's energy balance: Results for selected regions, J. Atmos. Sci., 5, 1157–1171, 1992. 8682

Rydberg, B.: Submillimeter-wave radiometric measurements of cirruscloud ice, Master's thesis, Chalmers University of Technology, Göteborg, Sweden, 2004. 8695

Stephens, G. L., Vane, D. G., Boain, R. J., Mace, G. G., Sassen, K., Wang, Z. E., Illingworth, A. J., O'Connor, E. J., Rossow, W. B., Durden, S. L., Miller, S., Austin, R. T., Benedetti, A., and Mitrescu, C.: The CloudSat mission and the A-train – A new dimension of space-based observations of clouds and precipitation, Bull. Am. Meteorol. Soc., 83, 1771–1790, 2002. 8684

Stubenrauch, C. J., Rossow, W. B., Chruy, F., Scott, N. A., and Chédin, A.: Clouds as seen by satellite sounders (3I) and imagers (ISCCP): I-Evaluation of cloud parameters, J. Climate, 12, 2189–2213, 1999. 8683

Urban, J., Lautié, N., Le Flochmoën, E., Jiménez, C., Eriksson, P., Dupuy, E., El Amraoui, L., Ekström, M., Frisk, U., Murtagh, D., de La Noë, J., Olberg, M., and Ricaud, P.: Odin/SMR limb observations of stratospheric trace gases: Level 2 processing of ClO, N_2O, O_3, and HNO_3., J. Geophys. Res., 110, D14307, doi:10.1029/2004JD005741, 2005. 8685, 8686

Winker, D. M. and Trepte, C. R.: Laminar cirrus observed near the tropical tropopause by LITE, Geophys. Res. Lett., 25, 3351–3354, 1998. 8683

Wu, D. L., Read, W. G., Dessler, A. E., Sherwood, S. C., and Jiang, J. H.: UARS/MLS cloud ice measurements: Implications for H_2O transport near the tropopause, J. Atmos. Sci., 62, 518–530, 2005. 8683, 8687

Wu, D. L., Jiang, J. H., and Davis, C. P.: EOS MLS cloud ice measurements and cloudy-sky radiative transfer model, IEEE Trans. Geosci. Remote Sensing, 44, 1156–1165, 2006. 8683

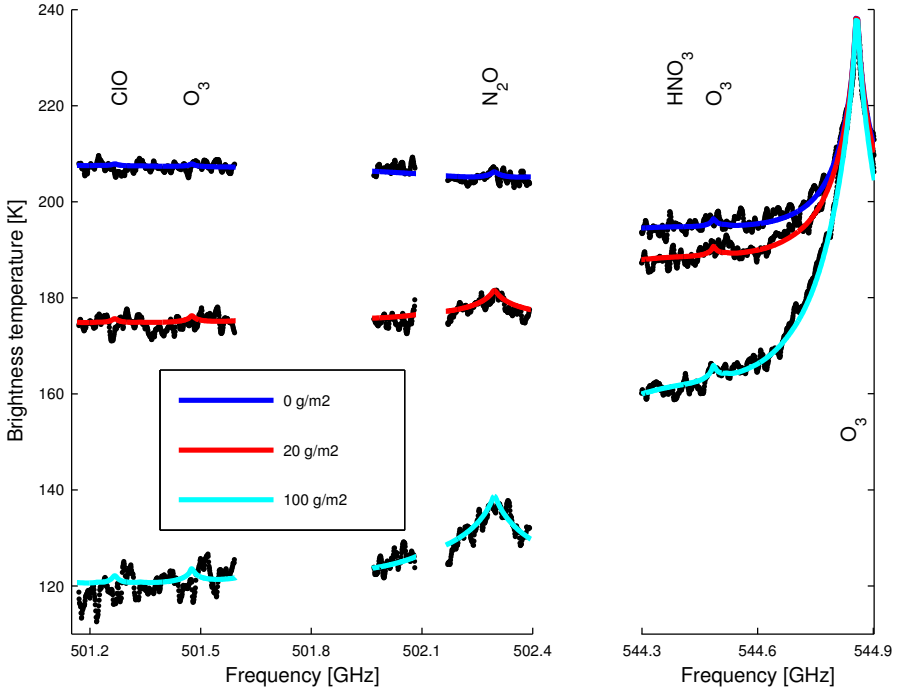

Fig. 1. Simulated and measured spectra of the Odin-SMR stratospheric mode. Tangent altitude is 7 km. Solid (coloured) lines are simulated spectra for different cloud ice columns. The assumed cloud layer extends between 12 and 15 km, with the ice vertically equally distributed. Dots (black) represent examples on measured spectra (at 10 MHz resolution, compared to the nominal value of 2 MHz).

ACPD
6, 8681–8712, 2006

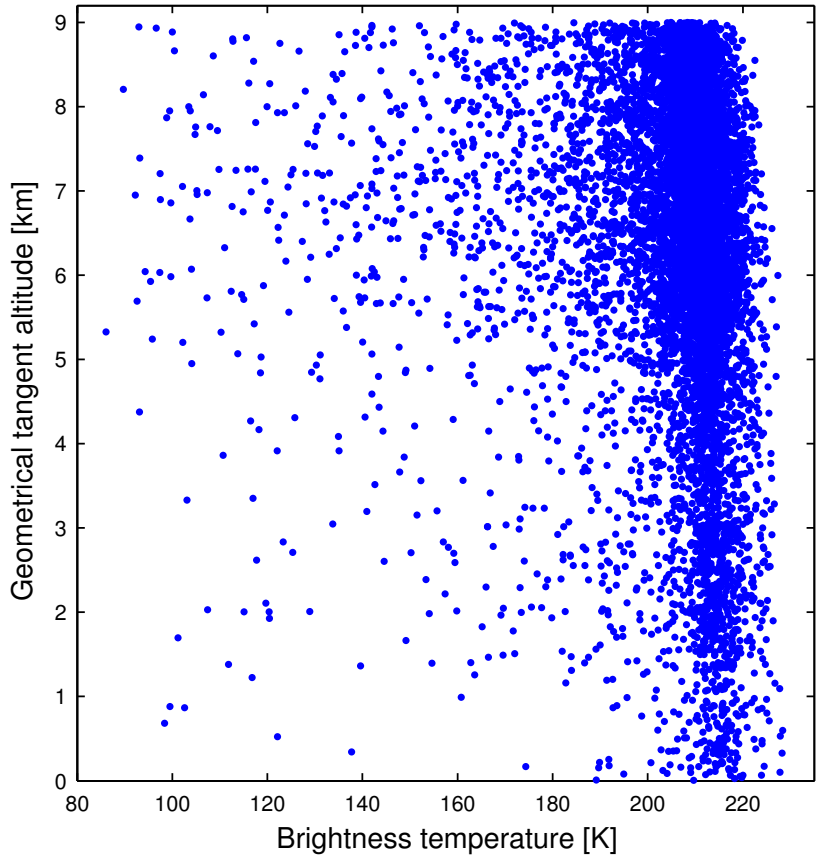

Fig. 2. Randomly selected values (10 000) from the 501 GHz part of the data set. The band of data values around 210 K corresponds to clear-sky conditions and relatively thin clouds, while lower brightness temperatures can only be caused by more dense ice clouds.

ACPD
6, 8681–8712, 2006

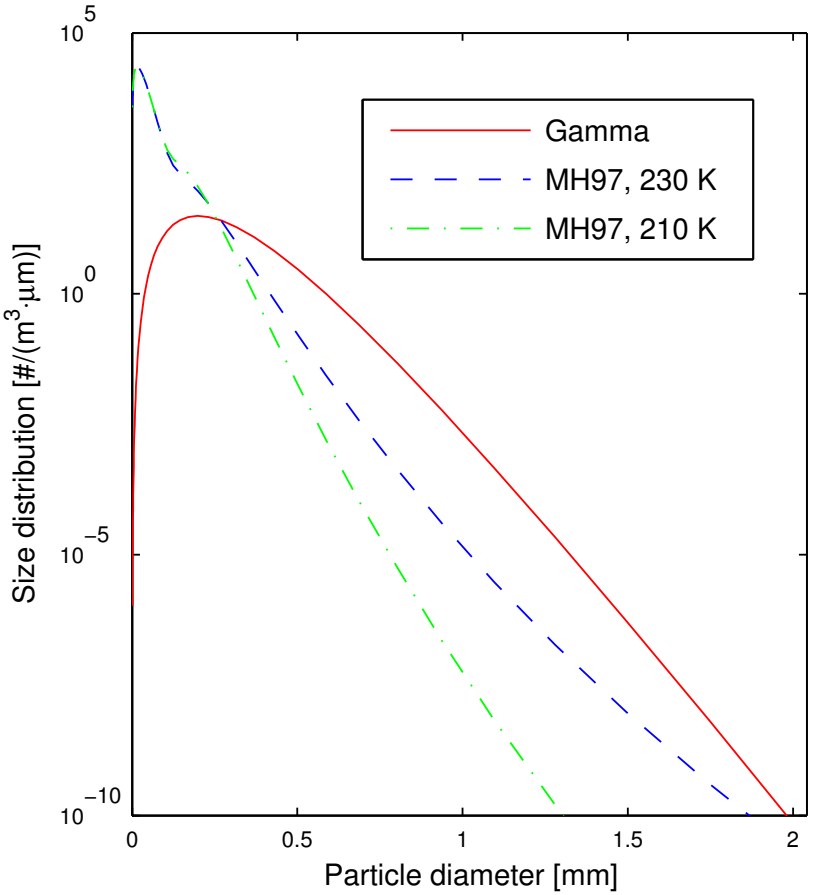

Fig. 3. Particle size distributions for an ice water content of 0.1 g/m^3. The parameterisation of McFarquhar and Heymsfield (1997), MH97, is shown for two temperatures. The shown gamma distribution is the one used for retrieval of minimum cloud ice columns.

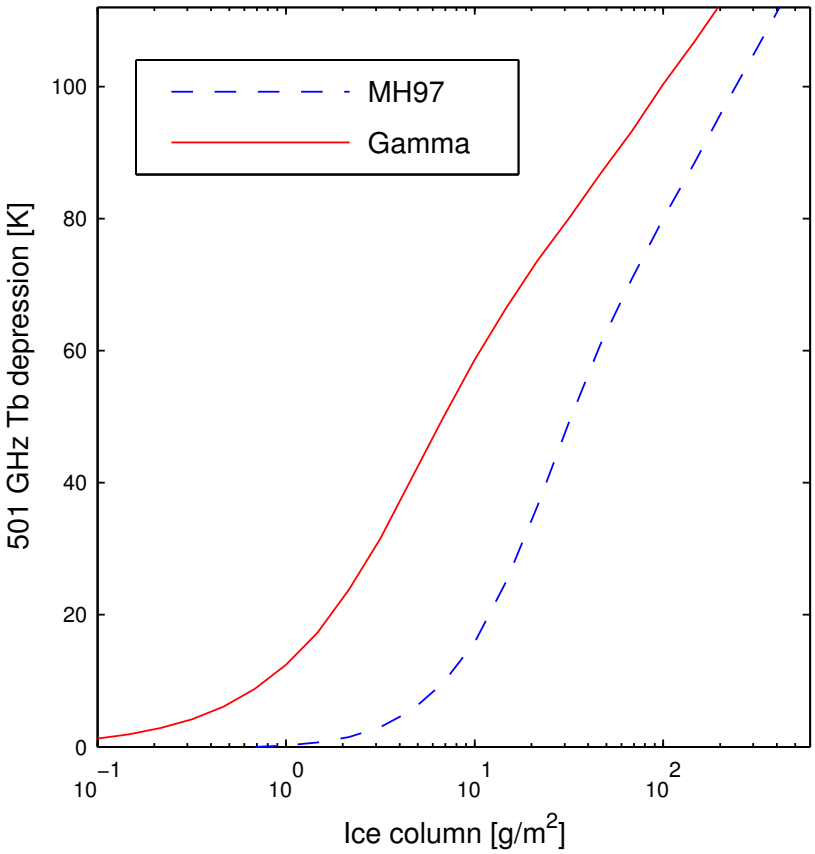

Fig. 4. Relationship between T_b depression and cloud ice amount, for two different particle size distributions. Simulations for 501 GHz, 7 km tangent altitude and cloud ice between 12 and 14 km.

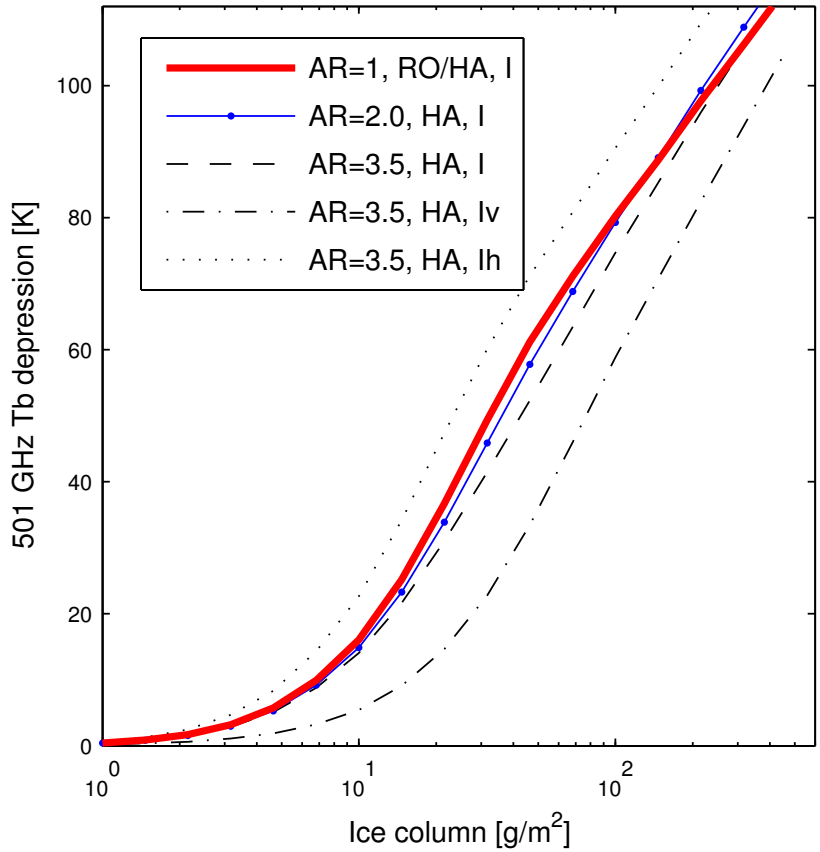

Fig. 5. Relationship between 501 GHz T_b depression and cloud ice amount, for different assumptions on particle shape and orientation where: AR = aspect ratio, RO = randomly oriented, HA = horizontally aligned, I = mean of I_v and I_h, and $I_{v/h}$ = intensity at vertical and horizontal polarisation, respectively. Simulations for MH97 PSD and cloud ice between 12 and 14 km.

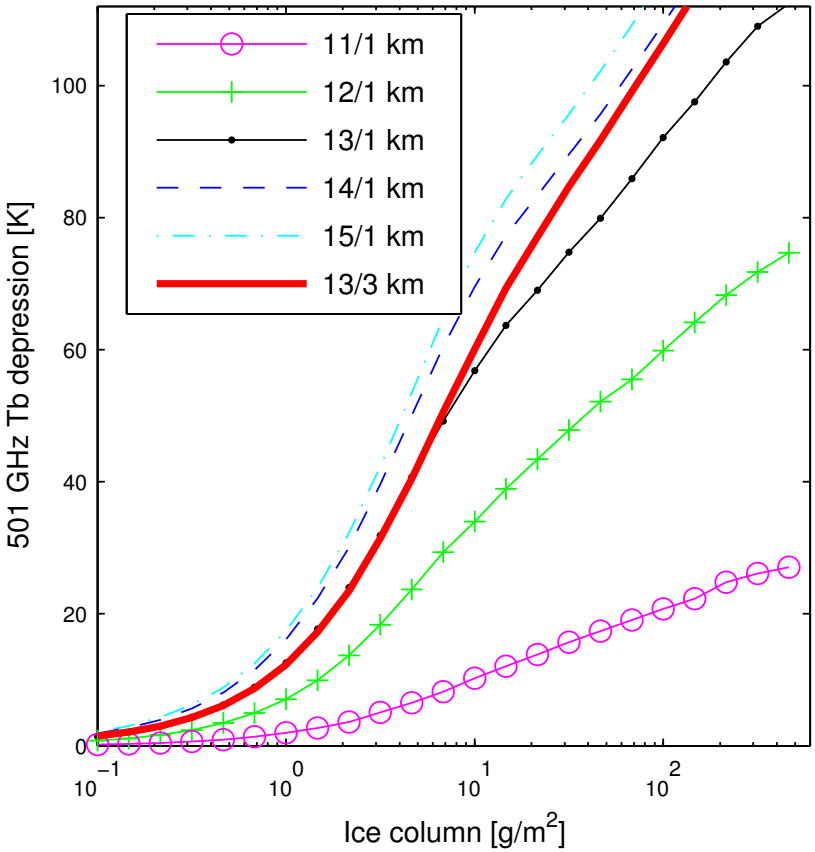

Fig. 6. Relationship between 501 GHz T_b depression and cloud ice amount, for different cloud altitudes and layer thicknesses. For example, the dotted line is for a cloud centre altitude of 13 km and a 1 km thick cloud layer. Simulations for 7 km tangent altitude and the 200 µm gamma distribution.

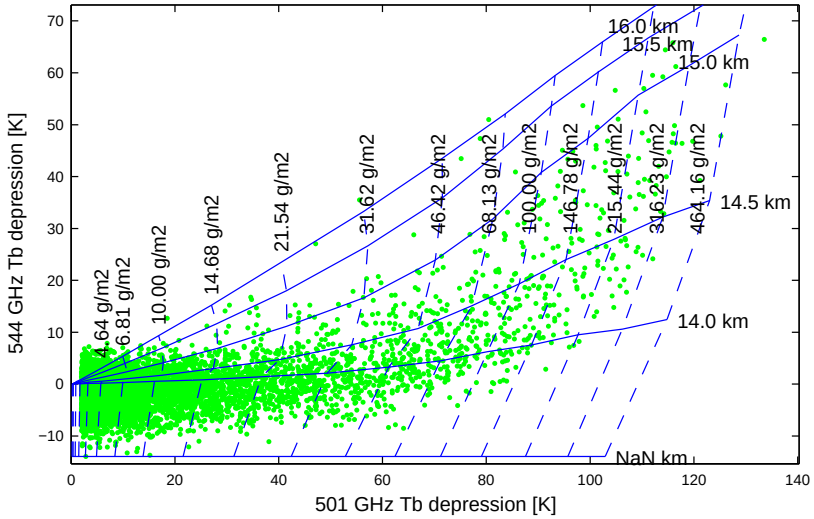

Fig. 7. Schematic of the retrieval algorithm. Dots (green) are measured values, given as estimated cloud ice induced brightness temperature depression at 501 and 544 GHz. Solid lines are the relationship between 501 and 544 GHz depressions found in simulations for constant cloud altitudes. Dashed lines show same relationship but for constant values of the cloud ice column. Clouds tops below about 14 km can not be altitude determined (see further Sect. 4.5). The MH97 PSD and a cloud layer thickness of 2 km are assumed. Data points with an apparent altitude above 16 km are discussed in Sect. 5.1.

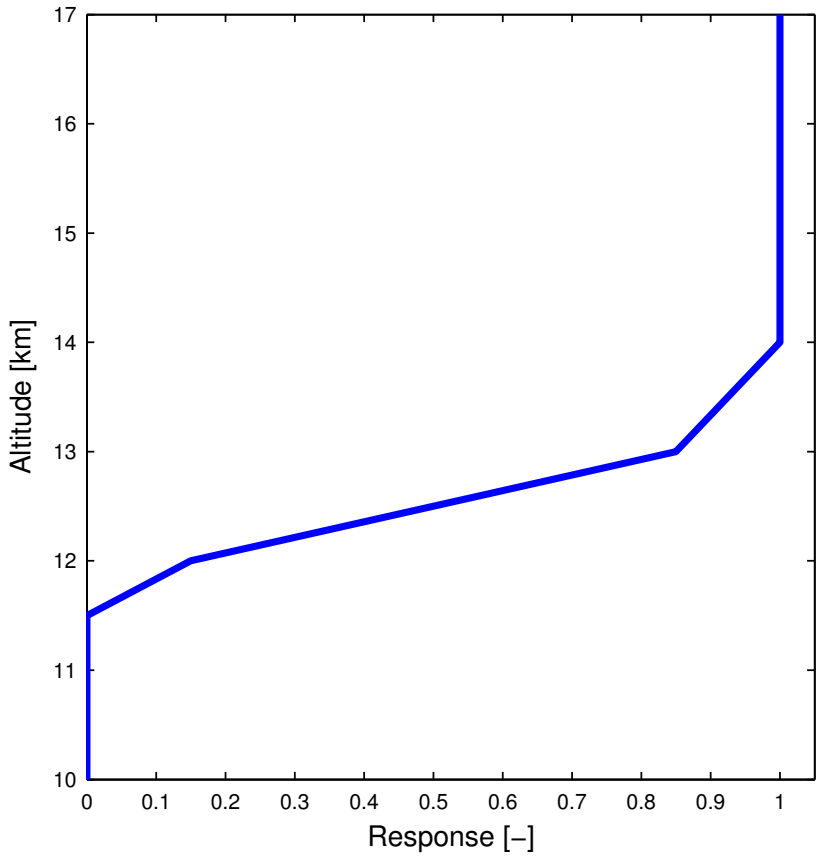

Fig. 8. Estimated altitude variation of cloud ice retrieval response. Data from other sources shall be weighted with this response before compared to Odin-SMR results obtained by the described retrieval algorithm.

ACPD
6, 8681–8712, 2006

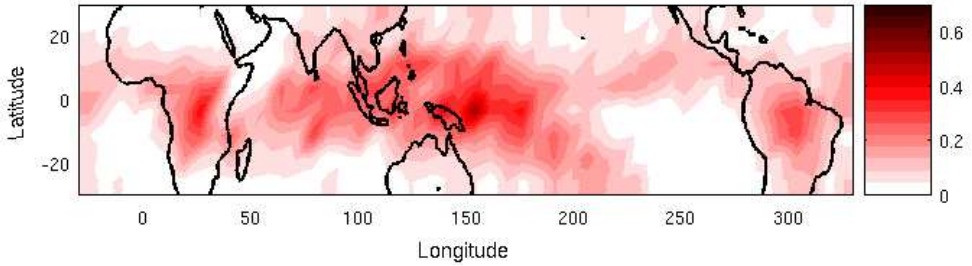

Fig. 9. Detection frequency for ice clouds above ~12 km, with a 5 K threshold for the 501 GHz ΔT_b. The data cover December 2001 to August 2004, with a somewhat uneven distribution between seasons. No distinction has been made between ascending and descending passages.

ACPD
6, 8681–8712, 2006

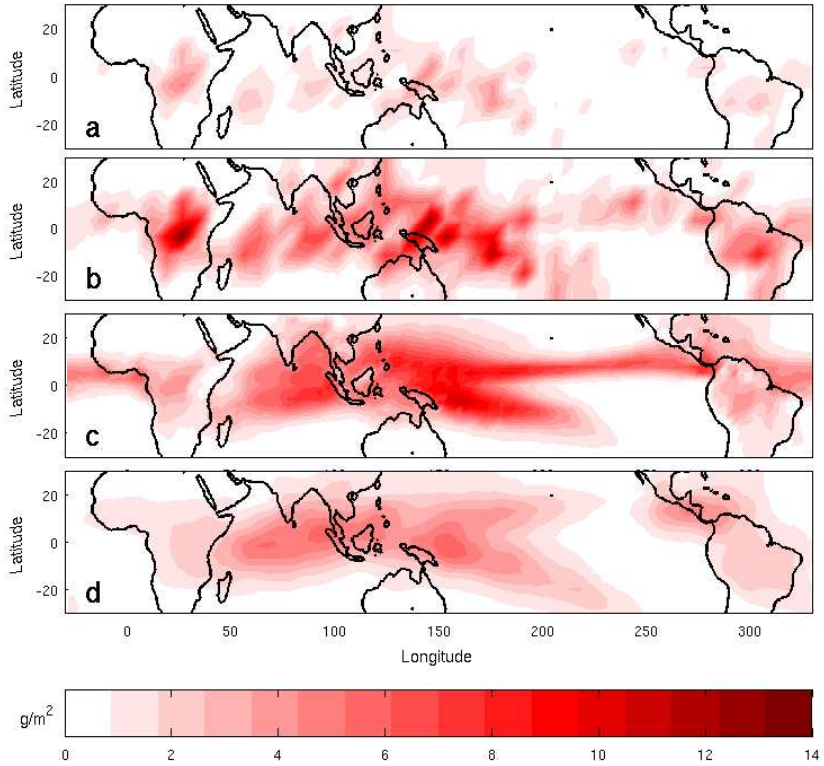

Fig. 10. Fields of partial ice columns: **(a)** Minimum Odin-SMR estimate (200 µm gamma PSD). **(b)** Best Odin-SMR estimate (MH97 PSD). **(c)** ECMWF, 2002–2004 mean. **d** ECHAM, 5 year climatological mean. Odin-SMR retrievals are averaged over December 2001–August 2004. ECMWF and ECHAM fields are weighted vertically with the function shown in Fig. 8.

ACPD
6, 8681–8712, 2006

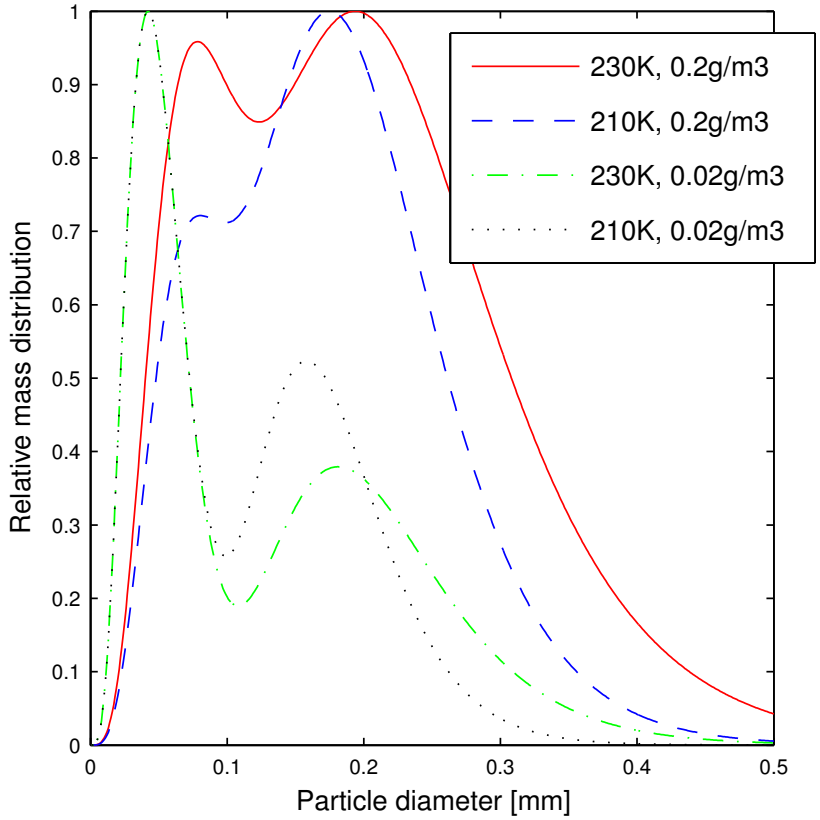

Fig. 11. Distribution of mass, as a function of particle size for different temperatures and ice water content. The MH97 PSD is assumed. Each distribution is normalised with its maximum value.